Available online at www.sciencedirect.com
ScienceDirect
Journal of the European Ceramic Society 27 (2007) 3391–3398
www.elsevier.com/locate/jeurceramsoc

Low elastic modulus metals for joint prosthesis: Tantalum and nickel–titanium foams

M. Arciniegas, C. Aparicio, J.M. Manero, F.J. Gil *

Biomedical and Biomechanical Research Centre (CREB), Technical University of Catalonia, Av. Diagonal. 647, 08028 Barcelona, Spain

Available online 30 April 2007

Abstract

In order to allow the ingrowth of the living tissue and increase the mechanical anchorage of the implant, Ta and NiTi foams were obtained with similar microstructure to cancellous bone and mechanically characterized. The Ta foams were produced by chemical vapour deposition and the NiTi foams by self-propagating high temperature synthesis (SHS). The mechanical and microestructural characterization was developed using a servohydraulic testing machine and microscopy techniques.

In both materials, pores in an appropriate range of sizes and interconnectivity were observed, comparable with the nature bone morphology. Moreover, the foams showed an excellent biomechanical compatibility and compressive fatigue limit. The fatigue endurance limit set at 10^8 cycles showed an approximate endurance limit of 7.5 and 13.2 MPa, for the NiTi and Ta foams, respectively. These results indicate that the studied materials provide an adequate structural support, showing mechanical properties similar to the cancellous bone, especially for the Ta foam.

Keywords: Mechanical properties; Biomedical applications

1. Introduction

In the biomaterials field, titanium alloys have extreme importance due to their excellent corrosion resistance and biocompatibility.[1,2] Moreover, alloys as the TiNi exhibit particular properties of shape memory, which promotes other interesting characteristics, such as high damping capacity, offered by the thermoelastic martensite phase; excellent wear behaviour provided by the α-phase when the martensitic start martensite, M_S, is near to room temperature and also, a low elastic modulus.[3–7]

Nevertheless, there is a controversial discussion about the Ni-ions release from the implant to the surrounding tissue, which promotes adverse reactions.[5,8–10] For that, Ni-free Ti alloys have been developed such as the Ti–4.4Ta–1.9Nb and Ti–29Nb–13Ta–4.6Zr alloys, which present a relative low elastic modulus and shape memory effects for some cases.[11,12]

It is important to notice that the low elastic modulus alloys are required to decrease the stress-shielding effect in bone-implant coupling, enhancing bone regeneration and avoiding resorption process. These alloys could be used in orthopedic, cardiovascular and dental applications, such as osteosynthesis plates, jaw plates and orthodontic archwires.[6]

However, it is in the orthopedic field where the called graft materials have a relevant importance in favour of the regeneration bone. The primary function of any orthopaedic graft material is to achieve an initial stabilization of the construct, while permitting a bone healing or bone ingrowth.[13] Many investigators have described the uses of different graft materials; local or iliac crest autograft or allograft, which sometimes work with other osteoconductive or osteinductive materials.[14,15]

Traditionally, the autograft has been the "gold standard" in orthopaedic reconstruction, but the ocurrence of donor-site morbidity has limited their applications. This, has promoted the use of some other osteoconductive or osteinductive materials such as cages, polymethyl-methacrylate or porous metallics grafts, porous metallic, as an alternative to the biological grafts.[13,14]

The porous materials have demonstrated their potential to allow rapid bone ingrowth. Therefore, this finding implies an important decrease in the time required for secondary stabilization of the implant by bone ingrowth. The most representative porous metallic materials are the tantalum and NiTi, which are used in a wide and varieties clinical applications including spine fusion. Different authors have reported mechanical properties of

* Corresponding author. Tel.: +34 934 016 708; fax: +34 934 016 706.
E-mail address: francesc.xavier.gil@upc.edu (F.J. Gil).

0955-2219/$ – see front matter © 2007 Elsevier Ltd. All rights reserved.
doi:10.1016/j.jeurceramsoc.2007.02.184

these materials, like Zardiackas et al.,[12] Li et al.[16] and Itin et al.[17] The biological responses have been reported by other authors as Bobyn et al.[13] and Gibson et al.[18] Nevertheless, more studies are required in order to improve the porous metals for biomedical applications, in fatigue behaviour, specially.

The purpose of the present paper is to produce Ta and NiTi porous materials, using the techniques of chemical vapour deposition/infiltration (CVD/CVI) and self-propagating high temperature synthesis (SHS), respectively, in order to obtain low elastic modulus, and to develop a complete mechanical characterization, to short- and long-term, of the mentioned materials.

Distribution and pore size measurements, compression tests, three-point bending test and compression fatigue tests in several samples of Ta and NiTi foams have been carried out. The results have been compared with the morphology and behaviour cancellous bone. In an attempt to improve our understanding of the mechanical behaviour of these porous materials, the failure mechanisms were studied by mean of scanning electron microscopy (SEM).

2. Material and methods

2.1. Sample preparation

The manufacture of the porous tantalum begins with the pyrolysis of a thermosetting polymer foam, precursor to obtain a low-density vitreous carbon skeleton, which has a repeating dodecahedron array of pores interconnected by smaller openings or portals. Commercially available pure tantalum is deposited into and about the carbon skeleton using CVD/CVI to create a porous metal construct.

The cylinders of porous NiTi were produced by SHS. This method is also called ignition synthesis and is based on the utilization of the exothermic heat of formation upon interaction of nickel and titanium. The increase of the temperature in the whole volume of the reacting system leads to a self-ignition that is similar to an explosion. In the reacting zones the maximum temperature values can be lower, equal or slightly higher than the melting point of NiTi. This method presents a good control of the porosity range, providing appropriately sized and interconnected pores, in order to create morphology close to that of the bone.[19] The chemical composition of the NiTi foams was equiatomic.

2.2. Pore size and distribution

Metallographic examination was developed by optical microscope (Olympus, 300 Japan) and scanning electron microscope (SEM, JEOL, 6400, Japan) equipped with Image Analysis Technique (Lynk, USA) on five of the cylinders studying different sections. From these observations, the pore size, the total porosity and isotropy were characterized.

2.3. Transformation temperatures of NiTi foam

The transformation temperatures were determined by means of differential scanning calorimetry (DSC, 2920 modulated DSC, TA Instruments) with heating and cooling ramps of 10 and 2 °C/min, respectively. M_s (martensite start) and M_f (martensite finish) are correspondingly, the starting and finishing temperatures of martensite formation upon cooling from the austenite phase. Similarly, A_s (austenite start) and A_f (austenite finish) are the starting and finishing temperatures of austenite formation upon heating from martensitic phase.

The calibration has been carried out with indium, and did not vary with the heating rate. After optimization in preliminary tests, a smaller rate upon cooling was used to ensure a flat baseline and consequently avoid inaccurate calculation of temperatures transformation and enthalpies.

2.4. Compression tests

Compression tests were performed according to ASTM 451 standard.[20,21] The test samples were cylinders with diameter of 10 mm and height 35 mm. Five specimens of each material were tested in compression at a cross-head speed of 10 mm/min. Load versus deflection was continuously monitored and recorded. These mechanical tests were performed using a servo-hydraulic testing machine (MTS-Bionix, USA). The tests were performed at 37 °C.

2.5. Three-point bending tests

Rectangular prismatic specimens of average size 3 mm × 4 mm × 30 mm were cut from as-prepared samples and polished with a #2000 grid blast. Three-point bending tests were performed using an Adamel Lhomargy® DY34 mechanical test machine fitted with a 100 N load cell. The assays were performed at 22 °C at a crosshead speed of 1 mm/min. The scheme of the test is shown in Fig. 1.

The elastic modulus, E, and the maximum bending strength (maximum stress at fracture), σ_{max}, were calculated by using Eqs. (1) and (2):

$$P = \left(\frac{48IE}{L^3}\right) d \Rightarrow E = \frac{PL^3}{48Id} \quad (1)$$

$$\sigma_{max} = \frac{3PL}{2bh^2} \quad (2)$$

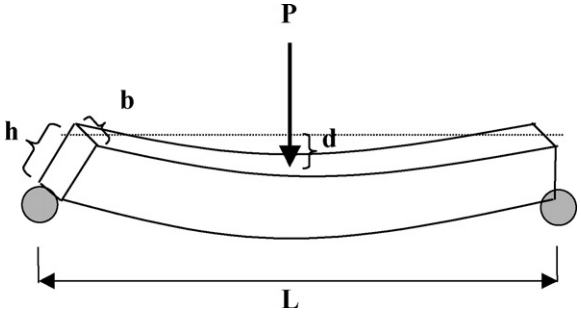

Fig. 1. Schematic diagram of the three-point bending test.

Table 1
Ion concentrations of simulated body fluid (SBF) and human blood plasma

	Concentration (mM)							
	Na^+	K^+	Mg^{2+}	Ca^{2+}	Cl^-	HCO^{3-}	HPO_4^{2-}	SO_4^{2-}
SBF	142.0	5.0	1.5	2.5	148.8	4.2	1.0	0.5
Human blood plasma	142.0	5.0	1.5	2.5	103.0	27.0	1.0	0.5

where P represent the load and I is the inertial moment with regard to the bh section calculated from Eq. (3):

$$I = \frac{bh^3}{12} \tag{3}$$

where L, d, b and h are the distances depicted in Fig. 1.

Eq. (1) was applied for the elastic region of the load versus displacement curves. To avoid changes in the slope of the linear part of the curves (elastic region), due to different values of inertial moment as a consequence of variations in the b and h dimensions of the pieces, the experimental load values were normalized considering a constant $I = 16\,mm^4$ for all the cases.

2.6. Compression fatigue

Cylindrical samples (diameter of 10 mm and height 35 mm) were cycled in compression to failure in simulated body fluid at 37 °C. The chemical composition of the simulated body fluid (SBF) is shown in Table 1.

The load was applied as a sinus wave function with a maximum load of −10 N. To generate S–N curves, the maximum load for successive tests was decreased at 5% intervals until samples survived 10^8 cycles. The testing machine used was a servohydrauilic MTS Bionix with a sensibility of 1 gf. The frequency was 2 Hz. Based upon initial data, at least four upper load values were chosen with at least three samples evaluated at each load level to establish the fatigue curve.

Failure was judged as having occurred when a final permanent vertical displacement of 5% from the maximum displacement at the onset of cyclical loading. The deformed and fractured specimens were observed by means of SEM.

All data were statistically analyzed using t-Student tests and one-way ANOVA tables, with Turkey's multiple comparison tests in order to evaluate statistically significant differences between sample groups. All statistical analyses were performed with Minitab™ software (Minitab release 13.0).

3. Results

The tantalum and NiTi foams exhibited an open porosity between 65–70% for the tantalum samples and 63–68% for the nickel–titanium ones. The pore sizes were 370–440 μm and 350–370 μm for tantalum and nickel–titanium, respectively. Besides, homogeneous pore distributions and isotropic structures were observed. These characteristics promote the capillary phenomena, and enhance the bone tissue ingrowth and good fixation of the implant.

As shown in Figs. 2 and 3, tantalum and NiTi foams possessed characteristics of three-dimensionally intercommunicated, permeable and open structure. Three orthogonal dimensions were observed with similar results indicating the isotropic pore growth structure. This is confirmed by micrographs of cross-sections showing no preferred direction for pore growth or coalescence (results not shown). The pore size parameters met the pore demand of porous biomaterial used for cancellous bone implant.

The compressive stress–strain curves of tantalum and NiTi foams are shown in Fig. 4. These curves are typical of cellular solid with open cells showing the three regimes of behaviour.[22–25]

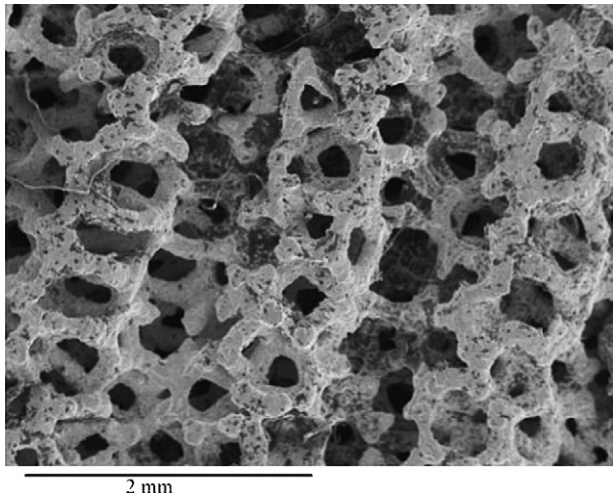

Fig. 2. SEM micrograph showing the structure of the tantalum foam.

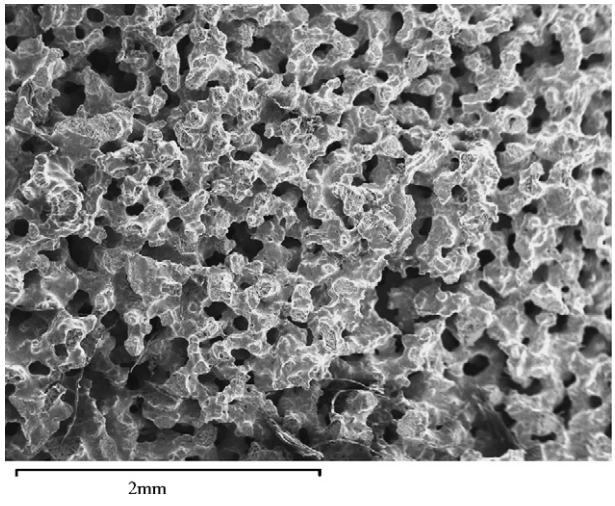

Fig. 3. SEM micrograph showing the structure of the nickel–titanium foam.

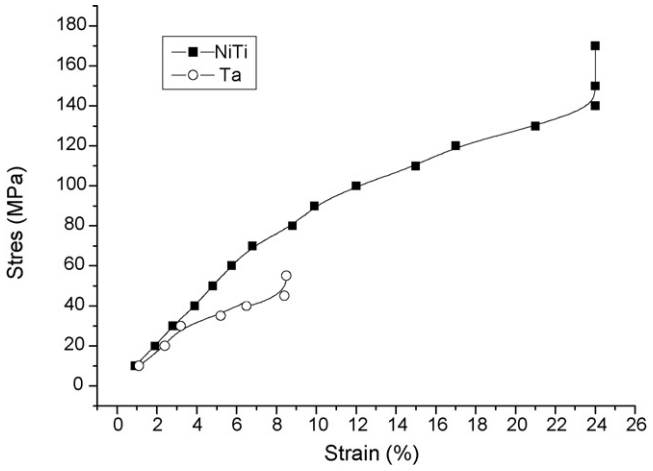

Fig. 4. Stress–strain curves of Ta and NiTi foams submitted at compression test.

1. *Linear elasticity*: At low relative densities, open-cell foams deform primarily by cell-wall bending.
2. *Non-linear elasticity and densification*: The deformation is still recoverable but it is non-linear. Elastic collapse in foams is caused by the elastic buckling of cell walls.
3. *Plastic collapse and densification*: Plastic collapse gives a long horizontal plateau to the stress–strain curve, through the strain is no longer recoverable. The failure is localized in a band transverse to the loading direction which propagates throughout the foam with increasing strain. The long stress plateau is exploited in foams for crash protection and energy absorbing systems. Plastic collapse in open-cell foam occurs when the moment exerted on the cell walls exceeds the fully plastic moment creating plastic hinges.

Progressive compressive collapse gives the long, horizontal plateau of the stress–strain curve which continues until opposing cell walls meet and touch, causing the stress to rise steeply. The collapse of the structure can be observed in Fig. 5 for NiTi foam after compression test.

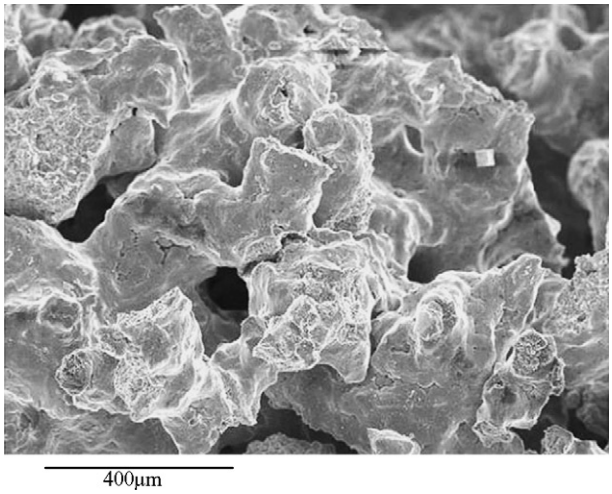

Fig. 5. SEM micrograph of the NiTi foam after a compression test, showing the collapse of the structure.

Table 2
Mechanical properties of the Ta and NiTi foams tested in compression, being E the Young's modulus, σ_0 the yield stress, σ_{max} the maximum strength and ε the strain to fracture

Material	E (GPa)	σ_0 (MPa)	σ_{max} (MPa)	ε (%)
Ta foam	1.15 ± 0.86	35.2 ± 0.8	71.2 ± 0.86	8.1 ± 1.8
NiTi foam	1.21 ± 0.31	101.3 ± 14.3	142.5 ± 29.3	23.0 ± 4.1
Cancellous bone	1.08 ± 0.86	15.2 ± 8.0	25.0 ± 8.1	7.1 ± 3.0

Results corresponding to cancellous bone are included for comparison.[21]

The results of the mechanical properties can be observed in Table 2. The results are very similar for the studied metallic foams and cancellous bone, especially for the tantalum foam. This fact is very interesting to the load transfer from implant to bone in order to minimize the stress shielding effect. The values of strength are higher for the NiTi foam than for the tantalum one and especially the results of strain to fracture are remarkably higher for the former, 23%, than for the latter, 8%.

Bending strength and bending rigidity were calculated and the results can be observed in Table 3. The bending rigidity, R, was defined as offset yield strength divided by elongation at offset yield. The R values are not significantly different; however, the NiTi foam shows a significantly higher strength value. If the obtained R values are compared with the R value of bone showed in Table 3, which corresponds to the trabecular bone, both studied materials present a remarkable difference. But if they are compared with the cortical bone, which is reported aprox. of 15 MPa/mm^2 the difference is less pronounced.[26–32] This mean that both materials present a higher stability for bending, which could generate pain in service due to their reduced elongation capacity; hence, further studies are required to improve the mechanical behaviour to serve in joint prosthesis.

Microscopy observation of the surfaces after bending revealed plastic deformation of the structure by elongation at the tensile side of the sample, but only very limited cracking of struts. A fracture of a strut of the tantalum foam is observed in Fig. 6.

The results of the DSC measurements for the untreated NiTi revealed an austenitic transformation with a broad peak of 30 °C width (A_s = 73 °C) and an enthalpy of ΔH = 2.28 J/g (see Fig. 7). The martensitic phase limits are found, respectively, at the temperatures of 69 °C (M_s) and 49.6 °C (M_f) with a ΔH = 2.26 J/g. The samples are in the martensite phase at body temperature. A single peak appeared during cooling cycle indicating that phase transformation from austenite to martensite occurred without the interposition of an R-phase.

Table 3
Mechanical properties of the Ta and NiTi foams tested in bending, being R the rigidity, σ_0 the yield stress and σ_{max} the maximum strength

Material	R (MPa/mm)	σ_0 (MPa)	σ_{max} (MPa)
Ta foam	46.7 ± 8.2	106.2 ± 25.3	125.4 ± 6.2
NiTi foam	42.2 ± 5.3	171.3 ± 32.1	192.3 ± 30.1
Cancellous bone	6.8 ± 3.1	5.1 ± 2.0	10.4 ± 4.8

Results corresponding to cancellous bone are included for comparison.

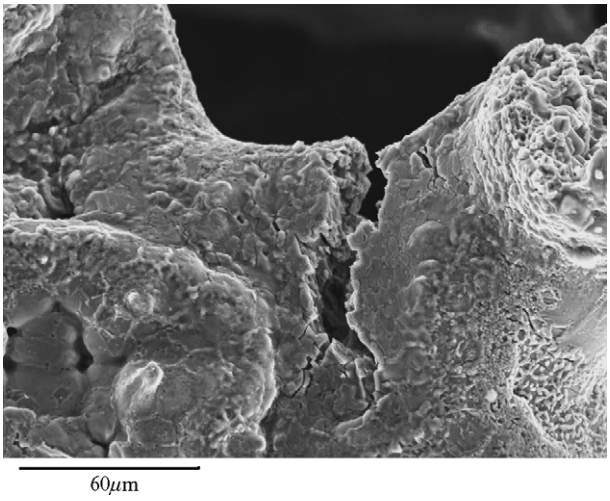

Fig. 6. SEM micrograph showing the fracture of the strut of tantalum foam.

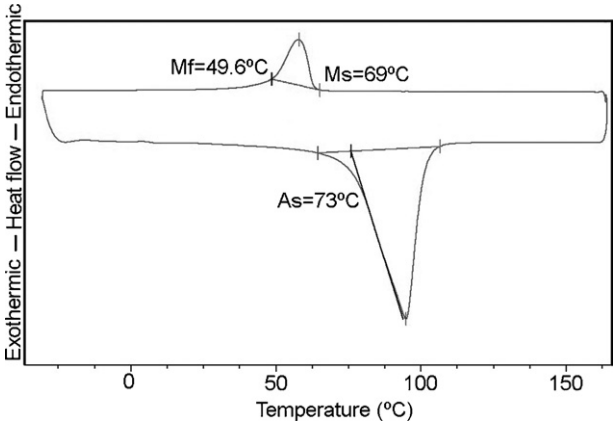

Fig. 7. DSC graph of the NiTi foam after heat treatment, which presents an Ms temperature of 69 °C.

The results of compressive fatigue were plotted as an *S*/*N* curve (see Fig. 8 for NiTi foam). SEM evaluation of fatigued samples showed cracking of the cylinders along the plane of maximum shear stress (45° from axis of applied load). Cracking

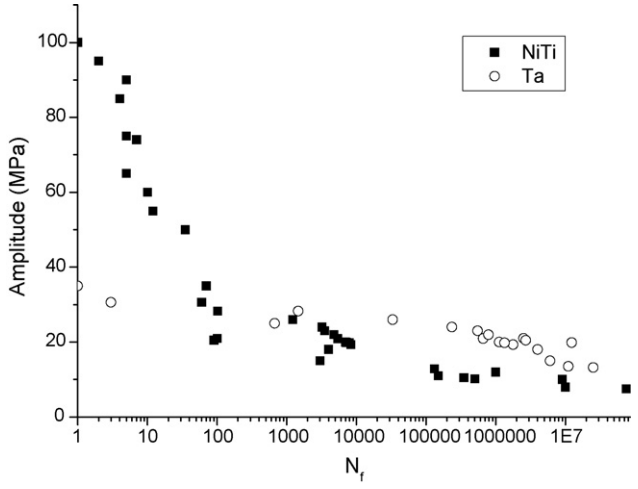

Fig. 8. *S–N* curves of the Ta and NiTi foams tested at compression fatigue.

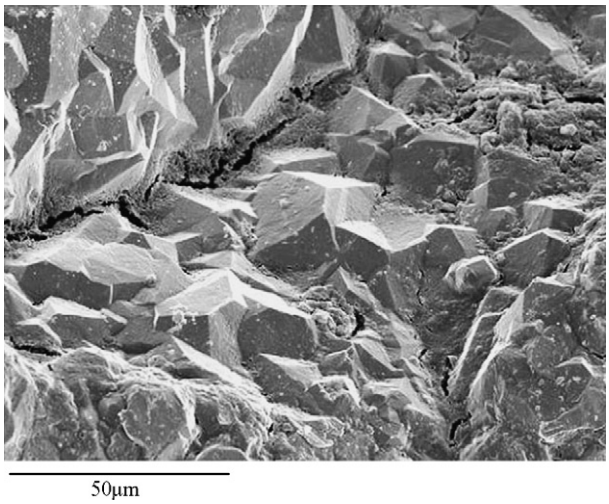

Fig. 9. SEM micrograph showing the fatigue cracks nucleated in the struts propagating by the structure of the Ta foam.

of the struts was concentrated along the crack path with fracture occurring at the strut junctions.

The fatigue endurance limit set at 10^8 cycles showed an approximate endurance limit of 7.5 MPa for the NiTi foam and 13.2 MPa for the tantalum one. Samples that failed in fatigue, regardless of load and number of cycles to failure, showed cracking as well as complete fracture of the struts. The fatigue cracks are nucleated in the struts and propagate through the structure, as can be observed in Fig. 9. Finally, the collapse of the structure by compressive fatigue is promoted when the cell walls get in contact and are compressed.

4. Discussion

4.1. Mechanical properties

For the cancellous bone, at a strain of about 1% the stress–strain curve becomes non-linear as the trabeculae start to deform irreversibly and crack. Beyond the peak, the stress–strain curve falls gradually as the trabeculae progressively fail by tearing and fracturing. As one would expect for a cellular solid, the density has a rofound influence in determining the stiffness and stress for cancellous bone. Others factors are important, as how the stress-induced orientation of the trabeculae gives large anisiotropies in properties: the longitudinal to transverse stiffness of cancellous bone in the human tibia, for instance, can differ by a factor of as much as 10.

Scaffold modulus data were comparable to trabecular bone. Specifically, the tantalum scaffolds closely matched the modulus and porosity of trabecular bone from the human vertebral bone. These data are similar to results for porous NiTi and appear to match bonelike characteristics better than other investigated bone replacement materials as coralline hydroxyapatite, calcium carbonate, and others.

When a bone replacement material is too stiff, this can result in an implant site that suffers from stress shielding, a condition in which the implant carries a disproportionate amount of load compared to the surrounding tissues. Stress shielding has been

implicated in bone resorption in tissues adjacent implants and subsequent implant loosening, which ultimately leads to failure of the implant. The lower modulus of the tantalum scaffold should prevent stress shielding in the area of the implant, and with time, bony ingrowth from the surrounding tissue should increase the structural stiffness and modulus of the implant such that it matches the mechanical properties of the bone it is intended to replace.

4.2. DSC measurements for the untreated NiTi

The cause of the high strain to fracture in this material is due to the thermoelastic martensitic transformation. Martensite phase appears as plates. The number of possible martensite plate orientations within one grain depends on the habit planes. For the thermoelastic martensitic transformation, several habit planes are possible and consequently many martensitic plate variants can occur, giving rise to a multivariant formation. The orientation taken by a growing martensite plate with respect to the orientation of its neighbour is the most energetically stable in that particular strain field. The strain associated with one variant compensates the strain in other variants. This phenomenon is called "self accommodation". In the absence of an external applied stress and when the volume change is negligible, the thermally induced martensitic transformation is characterized by random martensite plate variants. If a constant external applied uniaxial stress assists the thermally induced martensitic transformation, only a limited number of thermoelastic martensite variants are expected to grow, or in the case of self-accommodating formations, certain martensite plate variants will become dominant in the different groups, as it can be observed in Fig. 10. This will lead to an external macroscopic shape change.

"Rubber-like behaviour" is a name given to a type of behaviour that takes place at temperatures clearly below M_f. Samples composed completely of martensitic phase may be loaded until they reach a large strain, and when unloaded their initial shape is completely recovered. It seems that the process can be explained by the reorientation of the variants into the most stable direction and the coalescence between them. This is due to the low interfacial energy of the plates which makes the growth process totally reversible, and where some variants may grow at the expense of others. In fact, in the loading process, the growth of those variants that promote a better relaxation of the internal stress distribution caused by the external load is favoured. On unloading, with the consequent variation in the boundary conditions, the process is reversed and a reduction in the variants that have been developed is produced, until the initial self-accommodating structure is found. This behaviour is particularly sensitive to the thermomechanical treatment undergone by the sample.

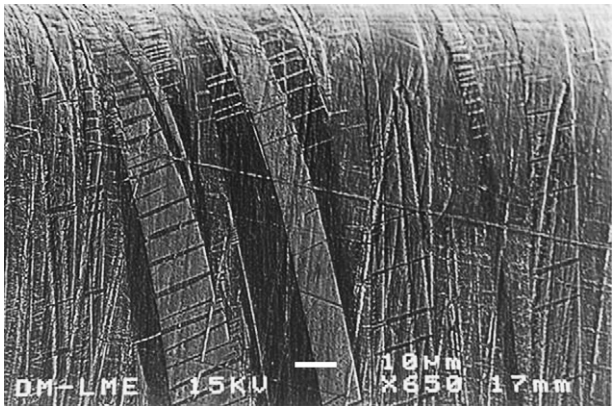

Fig. 10. Martensitic plates produced by quenching (a) from TiNi foam and the same martensitic plates oriented by the load applied (b).

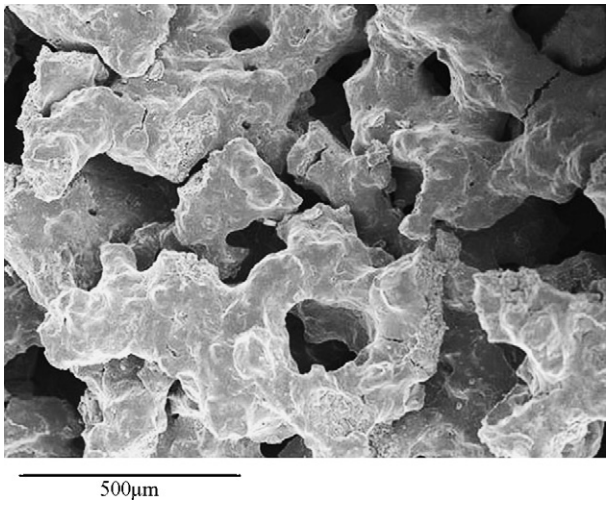

Fig. 11. SEM micrograph showing the fracture surface of the Ta foam tested at compression.

The mechanism of fracture was the same in both porous materials. SEM examination of the structure as a whole and of individual struts showed collapse of the structure orthogonal to the direction of load application as well as cracking of individual struts. These observations attest to ductility of the structure as a whole during deformation. The surface fracture revealed a typical cup/cone ductile fracture mode due to microvoid coales-

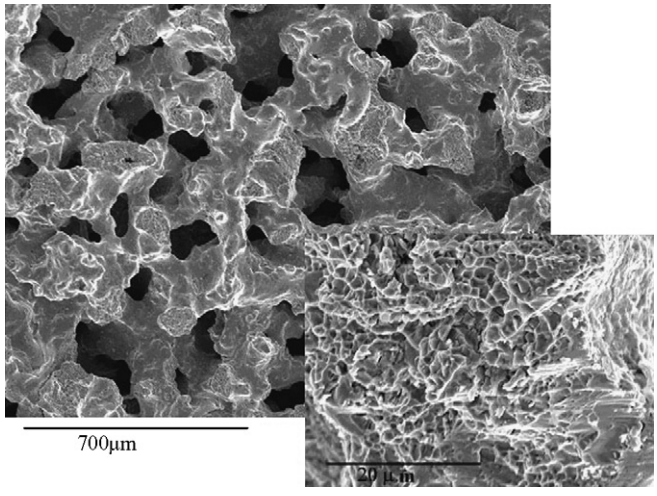

Fig. 12. SEM micrograph showing ductile fracture (detail of the Fig. 9 at higher magnification) from the Ta foam.

cence rather than a brittle fracture mode, as can be observed in Fig. 11 and with more detail in Fig. 12, for the tantalum foam.

Finally, it is important to notice that both studied materials present an adequate porous size and interconnectivity of them, if are compared with the nature bone. Despite of the high strength, excellent properties generated by shape memory effect and high strain to fracture exhibited by the studied NiTi foam, the Ta foam present a better elastic modulus and more comparable mechanical properties with the bone. For that, the Ta foam could be a better material for being used as joint prosthesis. Also this material is a Ni-free Ti alloy, which avoids the Ni-ion release to the surrounding tissue and then, the possibility of adverse reaction.

5. Conclusions

Tantalum and nickel–titanium porous materials have been obtained and studied with respect to its mechanical behaviour, by extensive microestructural analysis, using conventional techniques, in order to allow the ingrowth of the living tissue increasing the mechanical anchorage of the implant. The most relevant results of this study are:

(a) Both foams exhibited an open porosity between 65–70% for the tantalum samples and 63–68% for the nickel–titanium ones.
(b) The mechanical properties obtained from the studied metallic foams, were very similar to the cancellous bone, especially those obtained from the tantalum foam.
(c) The NiTi foam presented strength values higher than the Ta one, and the results of strain to fracture are remarkably higher for the former, 23%, than for the latter, 8%.
(d) The fatigue endurance limit set at 108 cycles showed an approximate endurance limit of 7.5 and 13.2 MPa for the NiTi and Ta foams, respectively.
(e) The failure mechanisms, studied by SEM, showed a collapse of the structure orthogonal to the direction of load application as well as cracking of individual struts showing in both materials.

Acknowledgements

The authors wish to thank Spanish Ministry of Science and Technology for financial support through grants MAT2003-08165 and MAT2005-07244.

References

1. Collier, D. P., Mayor, M. B. and Chae, J. C., Macroscopic and microscopic evidence of prosthetic fixation with porous-coated materials. *Clin. Orthop.*, 1998, **3**, 249–262.
2. Cook, S. D., Barrack, R. L., Thomas, K. A. and Haddad, R. J., Quantitative analysis of tissue growth into human porous total hip components. *J. Arthroplasty*, 1988, **3**, 249–262.
3. Cook, S. D., Barrack, R. L., Thomas, K. A. and Haddad, R. J., Tissue growth into porous primary and revision femoral stems. *J. Arthroplasty*, 1991, **6**(Suppl), 37–46.
4. Engh, C. A., Hooten, J. P. and Zettl-Schaffer, K. F., Evaluation of bone ingrowth in proximally and extensively porous-coated anatomic medullary locking prostheses retrieved at autopsy. *J. Bone Joint Surg. (Am.)*, 1995, **77A**, 903–910.
5. Engh, C. A., Zettl-Schaffer, K. F. and Kukita, Y., Histological and radiographic assessment of well functioning porous-coated acetabular components: a human post-mortem retrieval study. *J. Bone Joint Surg. (Am.)*, 1993, **75A**, 814–824.
6. McGree, T. D., Graves, M. A., Twende, K. S. and Niederauer, G. G., A biologically active ceramic material with enduring strength. In *Encyclopedic Handbook of Biomaterial and Bioengineering. Part B. Applications*, *vol. 1*, ed. D. L. Wise. Marcel Dekker, New York, 1995.
7. Gresser, J. D., Lewanndrowski, K. U., Trantolo, D. J. and Wise, D. L., Soluble calcium salts in bioresorbabl bone grafts. In *Biomaterials Engineering and Devices: Human Applications*, ed. D. L. Wise. Humana, Totowa, New Jersey, 2000.
8. Ginebra, M. P., Driessens, F. C. M. and Planell, J. A., Effect of the particle size on the micro and nanostructural features of calcium phosphate cement: a kinetic analysis. *Biomaterials*, 2004, **25**, 3453–3462.
9. Navarro, M., Ginebra, M. P., Planell, J. A., Zeppetelli, S. and Ambrosio, L., Development and cell response of a new biodegradable composite Scaffold for guided bone regeneration. *J. Mater. Sci. Mater. Med.*, 2004, **15**, 417–420.
10. Gil, F. J., Manero, J. M. and Planell, J. A., Relevant aspects in the clinical applications of NiTi shape memory alloys. *J. Mater. Sci. Mater. Med.*, 1996, **7**, 403–406.
11. Hin, V. I., Gjunter, V. E., Shabalovskaya, S. A. and Sachdeva, R. C. L., Medical properties and shape memory porous nitinol. *Mater. Charact.*, 1994, **32**, 179–187.
12. Zardiackas, L. D., Parsell, D. E., Dillon, L. D., Mitchell, D. W., Nunnery, L. A. and Poggie, R., Structure, metallurgy, and mechanical properties of a porous tantalum foam. *J. Biomed. Mater. Res. (Appl. Biomater.)*, 2001, **58**, 180–187.
13. Bobyn, J. D., Stackpool, G. J., Hacking, S. A., Tanzer, M. and Krygier, J. J., Characteristics of bone ingrowth and interface mechanics of a new porous tantalum biomaterial. *J. Bone Joint Surg. (Br.)*, 1999, **81B**, 907–914.
14. Hernández, R., Polizu, S., Turenne, S. and Yahia, L'H., Characteristics of porous nickel–titanium alloys for medical applications. *Bio-Med. Mater. Eng.*, 2002, **12**, 37–45.
15. Ayers, R. A., Bateman, T. A. and Simske, S. J., Porous NiTi and a material for bone engineering, basic properties. In *Shape Memory Implants*, ed. L. H. Yahia. Springer-Verlag, New York, 2000.
16. Li, Y. H., Rong, L. J. and Li, Y. Y., Compressive property of porous NiTi alloy synthesized by combustion synthesis. *J. Alloys Compd.*, 2001, **345**, 259–325.
17. Itin, V. H., Gjunter, V. E. and Shabalovskaya, S. A., Mechanical properties and shape memory of porous nitinol. *Mater. Charact.*, 1994, **32**, 179–182.
18. Gibson, L. J. and Ashby, M. F., *Cellular Solids*. Cambridge University Press, Cambridge, UK, 1997.
19. Williams, J. C. and Lewis, J. L., Properties and an anisotropic model of cancellous bone from the proximal tibial epiphysis. *J. Biomech. Eng.*, 1982, **104**, 50–54.
20. Wright, T. M. and Hayes, W. C., Fracture mechanics parameters for compact bone-effects of density and specimen thickness. *J. Biomech.*, 1977, **10**, 419–423.
21. Odgaarg, A. and Linde, F., The underestimation of Young's modulus in compressive testing of cancellous bone specimens. *J. Biomech.*, 1991, **24**, 691–698.
22. Linde, F., Norgaard, P., Hvid, I., Odgaard, A. and Soballe, K., Mechanical properties of trabecular bone. Dependency on strain rate. *J. Biomech.*, 1991, **24**, 803–809.
23. Slivka, M. A., Leatherbuy, N. C., Kieswetter, K. and Niederauer, G. G., Porous, resorbable, fiber-reinforced scaffolds tailored for articular cartilage repair. *Tissue Eng.*, 2001, **7**, 767–780.
24. Thomson, R. C., Yaszemski, M. J., Powers, J. M. and MIkos, A. G., Fabrication of biodegradable polymer scaffolds to engineer trabecular bone. *J. Biomater. Sci. Polym. Ed.*, 1995, **7**, 23–38.
25. Shimko, D. A., Shimko, V. F., Sander, E. A., Dickson, K. F. and Nauman, E. A., Effect of porosity on the fluid flow characteristics and mechanical properties of tantalum scaffolds. *J. Biomed. Mater. Res. Part B: Appl. Biomater.*, 2005, **73B**, 315–324.

26. Gil, F. J., Manero, J. M. and Planell, J. A., Relevant aspects in the clinical applications of NiTi shape memory alloys. *J. Mater. Sci.: Mater. Med.*, 1996, **7**, 403–406.
27. Gil, F. J., Libenson, C. and Planell, J. A., Differences in the pseudoelasticity behaviour of nickel–titanium orthodontic wires. *J. Mater. Sci.: Mater. Med.*, 1993, **4**, 281–284.
28. Delaey, L. and Thienel, J., In *Shape Memory Effects in Alloys*, ed. J. Perkins. Plenum, New York, 1975, pp. 124–156.
29. Barceló, G., Rapacioli, R. and Ahlers, M., The rubber effect in Cu–Zn–Al martensite. *Scripta Met.*, 1978, **12**, 1069–1074.
30. Ahlers, M., Barceló, G. and Rapacioli, R., A model for the rubber-like behaviour in Cu–Zn–Al martensites. *Scripta Met.*, 1978, **12**, 1075–1078.
31. James, D. W., High damping for engineering applications. *Mater. Sci. Eng.*, 1969, **4**, 13–17.
32. Lin, H. C., Damping characteristics of TiNi shape memory alloys. *Metall. Trans. A*, 1993, **24**, 2189–2197.